Steel Reinforced Grout under uniaxial load: experimental evidences and numerical modelling

Marialaura Malena[a], Marialuigia Sangirardi[a], Gianmarco de Felice[a,*]

[a] *Department of Engineering, Roma Tre University, Via Vito Volterra 62, 00146 Rome, Italy*

Abstract

The use of composite materials as structural retrofitting tools has been strongly encouraged by their capability of improving structural performance causing minimum invasiveness and reduced weight increment.

For decades, Fiber Reinforced Polymers were considered the most suitable composites for retrofitting purposes but, more recently, technological issues have revealed some drawbacks, mainly related to their applications on masonry substrates. A viable alternative is represented by Fabric Reinforced Cementitious Matrix (FRCM), a class of composites made of high-strength textiles with inorganic matrix. Among them, Steel Reinforced Grout (SRG) systems, made of Ultra High Tensile Strength Steel cords embedded in cement or lime-based mortar, are widely used, particularly for repairing or strengthening masonry constructions.

Qualification tests and acceptance criteria of these composites have been recently proposed. Numerical simulations of current available experimental test procedures need to be performed to provide a more rigorous insight into the mechanisms that control the composite response up to failure, namely the brittle cracking of the matrix, the ductile response of the steel and the debonding at the mortar-fabric interface. These aspects not only affect the microscale, but are indeed responsible for the macroscopic response of the composite.

In this work a finite element simulation of direct tensile tests on SRG systems is presented. Two different gripping methods have been considered, the clamping-grip and the clevis-grip, which identify two standardized test procedures according to RILEM and ACI respectively. Numerical results are first compared with the experimental outcomes to assess the accuracy of the model in reproducing the quantitative and qualitative aspects of composite tensile response. Then, the effects of different boundary conditions on failure mechanisms are investigated, analysing damage and stress patterns in the constituents.

Keywords: SRG, Tensile tests, Numerical modelling, Experimental tests.

*Corresponding author

Email addresses: `marialaura.malena@uniroma3.it` (Marialaura Malena), `marialuigia.sangirardi@uniroma3.it` (Marialuigia Sangirardi), `gianmarco.defelice@uniroma3.it` (Gianmarco de Felice)

1. Introduction

Fabric Reinforced Cementitious Matrix (FRCM), made of high-strength textiles embedded in an inorganic matrix, are nowadays largely considered an efficient and sustainable retrofitting tool. Their mechanical characterisation is generally based on tensile tests of FRCM specimens, used both for classifying and comparing different matrix and textile combinations and for providing useful design values to engineers. The mechanical properties obtained from separate tests on fabric and matrix cannot be directly employed to obtain the mechanical properties of the composite material [1]. This is owed to the interaction between the brittle matrix with the textile, resulting in multiple cracking of the matrix, relative slip between the fibres and the matrix and, eventually, in rupture of the fibres. The setup adopted for the tensile test for this type of composites plays a decisive role in capturing their characteristic stress-strain behaviour.

Different setups for tensile testing, mainly differing in specimen morphology, clamping method and measurement technique, have been proposed in the literature. The most commonly adopted specimen types are the coupons, i.e. rectangular prism [2, 3] or the dumbbell [1]. Clamping methods for rectangular prisms include direct clamping by hydraulic or pneumatic wedges (referred to as clamping-grip) [4], bonding of steel or aluminum plates to the specimen ends and connecting the plates to the machine through hinge joints (referred to as clevis-grip) [5, 6, 7] and drilling of holes in the specimen ends and clamping of the steel rods inserted through the holes [3]. This last technique is also applicable to dumbbell specimens [1]. During testing the axial deformation can be measured by using the stroke of the machine, by either Linear Variable Differential Transformers (LVDTs) or extensometers applied on the specimen.

Each test setup described can be associated with a different control mode: tensile tests on Textile Reinforced Concrete specimens were usually conducted under force control [8], while tensile tests on FRCM are generally performed in displacement control by increasing the stroke of the machine. It should be noted that the control mode and rate adopted may have a non negligible influence on the load response obtained in both cases of static [9] or dynamic loads [10]. Unfortunately, studies available in the literature do not provide a clear understanding of the influence of the adopted rate. It is worth noting that, results obtained by different setups cannot be easily compared [5, 8]. More in general, results of tensile tests on FRCM composite materials are affected by the presence of fabrication defects and measurement technique employed [3]. Furthermore, several parameters, such as specimen geometry, textile geometry, manufacturing or curing process, differential shrinkage and coating or impregnation of textiles affect the behavior of the composite material and need to be properly investigated [2, 1, 8]. In same cases, aiming at minimising systematic error deriving, for example, from manufacturing or curing process, the specimens cut from greater plates, can be systematically tiled [8].

In this paper, two standardized tensile testing procedures adopted respectively by RILEM and ACI in the characterization of steel reinforced grout systems are analysed in detail: the clamping-grip proposed in [11] and the clevis-grip setup recommended by [12] for acceptance criteria. A particular class of FRCM systems named Steel Reinforced Grout (SRG) is considered, made of unidirectional ultra-high tensile strength steel cords embedded in a cementitious matrix. A finite element model based on a micro-mechanical approach in which both, the matrix and the steel cords, are discretized with three-dimensional elements, is used to simulate the tensile tests of SRG systems. A brittle strain-softening behaviour for the matrix was adopted, in which the stress-strain curve is calibrated from experimental tensile tests on SRG specimens, aiming at including the typical tension stiffening phenomenon in the overall response [2, 1, 3, 8, 4]. It is worth noting that in several studies a brittle behaviour without strain-softening is assumed for the mortar and the tension stiffening effect is accounted in a properly calibrated cohesive stress-slip law at matrix-fibre interface [13, 14, 15]. Conversely, in the present case the cohesive stress-slip law at matrix-fibre interface is used only to represent the macroscopic debonding between the fabric and the matrix at failure.

The obtained numerical results have been compared with the experimental outcomes for both gripping configurations, with the aim of reproducing the mechanical behaviour of the composite under tensile load with different boundary conditions.

Some sensitivity analyses, introducing the effect of manufacturing defects in the case of clamping-grip setup, have been carried out, aiming at explaining some scatter in the experimental results.

The paper is organised as follows: in Section 2 and 3 the tensile behaviour of SRG composites is described and the testing methods are briefly presented. In Section 4 the finite element model is introduced providing the details on adopted mechanical properties and boundary conditions. Finally, the results of the analyses are presented in Section 5, highlighting the capability of the model in reproducing the experimental responses and discussing the features of the clamping-grip and the clevis-grip testing procedures.

2. Overview of direct tensile tests on FRCM

In this section the two experimental setups used for the mechanical characterization of FRCM systems are described.

The setups essentially differ in the adopted gripping method, i.e. in how the load is transferred from the machine to the specimen and, consequently, in the stress pattern that develops and affects the tensile behaviour during the test up to failure. Figure 1 reports the clamping-grip (a) and the clevis-grip (b) setups.

The tests performed with clamping-grips allow a complete mechanical characterization of the composite up to the tensile failure of the reinforcement. In this case, the ends of the specimen are fastened thanks to a lateral pressure provided by the wedges, so that both compression and shear are transferred, allowing a complete mechanical characterization up to failure. Clevis-grip tensile

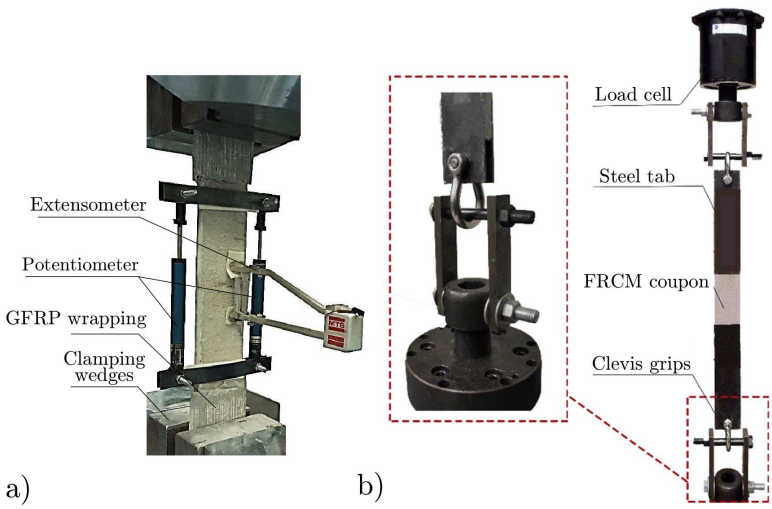

Figure 1: Experimental setup for direct tensile test on SRG specimens: a) clamping-grip setup and b) clevis-grip setup.

tests are thought to represent the behaviour of the composite in its installation conditions, i.e. without lateral pressure. Generally, the resisting mechanism is driven by the bond between the textile and the matrix, therefore only shear stresses are transferred between fabric and mortar, and failure is attained because of slippage of the textile.

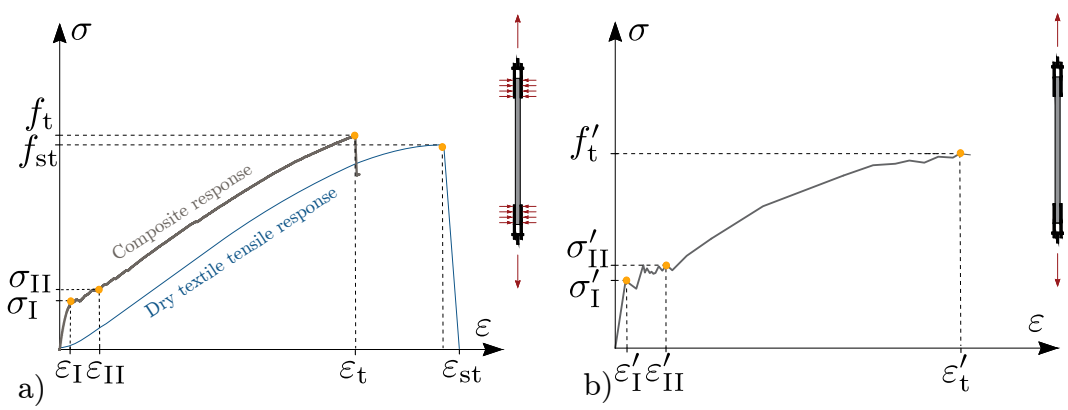

Figure 2: Tensile stress-strain response curve: a) clamping-grip setup and b) clevis-grip setup.

2.1. Clamping-grip setup

RILEM TC 232-TDT Recommendation [11], originally developed for Textile Reinforced Concrete (TRC), is the reference standard for the mechanical characterization of SRG strengthening systems in European countries.

The tensile test is performed on prismatic specimens with rectangular cross section, usually comprising one layer of fabric between two layers of mortar, placed with the fibres parallel to the longitudinal axis of the specimen and symmetrically with respect to both width and thickness. Specimens can be either manufactured individually in wooden, steel or glass moulds or cut to size from larger plates. Attention must be paid when placing the textile to avoid misalignments and non-planarity of the reinforcement. The coupons have to be de-moulded and then cured for 28 days at minimum 95% relative humidity.

Once the specimen is placed between the wedges of the testing machine, a lateral pressure is applied at the clamped edges through an hydraulic system and then the test is carried out under displacement control. Stresses are conventionally calculated dividing the axial load by the textile area and strains are measured by an extensometer or derived by the displacement measured by a transducer.

The behaviour shown during this test is reported in Figure 2, where the typical tri-staged response is schematically outlined. The first stage represents the uncracked, almost linear response of the composite. During this phase, both stiffness and load bearing capacity are controlled by the matrix properties, improved by the presence of fibres. The formation of the first crack in the matrix $(\sigma_{\mathrm{I}}, \varepsilon_{\mathrm{I}})$ marks the transition to the second stage, characterized by a progressive development of the crack pattern accompanied by a marked stiffness decay up to the point $(\sigma_{\mathrm{II}}, \varepsilon_{\mathrm{II}})$. At the third stage, the cracks are stabilized and increase their width, resulting in a higher stiffness with respect to the previous stage. The load bearing capacity of the composite is mainly due to the tensile strength of the textile and to the stiffening effect of uncracked portions of matrix. As highlighted in [1] when a regular multiple crack pattern appears a higher load bearing capacity is reached.

The response curve of the composite may show higher values of the peak stress (f_{t}) if compared to the dry textile (f_{st}) (Figure 2a). This can be attributed to various reasons: geometrical and technological characteristics of fabric and mortar can prompt interlocking and, consequently, enhance the development of tension stiffening (similarly to reinforced concrete elements). Moreover, being embedded in the matrix, the steel cords can benefit from a more efficient stress redistribution. The difference in peak strength can indeed be interpreted as an effect of the different boundary conditions of steel cords, rather than an apparent increase of the tensile strength of the composite.

2.2. Clevis-grip setup

Annex A of AC434 [12] provides instructions to perform direct tensile tests with a clevis-grip setup. The tests are carried out, as for the case of clamping-grip setup, on prismatic specimens, manufactured following the same process already explained in the previous paragraph. In this case, however, no lateral pressure is applied at the gripping areas; two steel tabs are placed at both ends of each coupon, fixed with high-strength epoxy glue. The clevis-grips are attached by a pin to the ends of the steel tabs to avoid load misalignments. Tensile tests are then performed under displacement control using a universal screw-driven

test frame and the axial load is transferred from the tabs to the matrix and from the matrix to the fabric at both sides of the coupon only through bond interaction. Load, strains and stresses are measured analogously to the case of clamping-grip setup. As the load transferred is controlled by the bond between the matrix and the reinforcement in the gripping area, the results of the tests may be affected by the bonded length of the steel tabs.

The stress-strain tensile response curve of the composite coupon under clevis-grip conditions displays a similar three-staged behaviour: an initial uncracked stage, followed by a crack-development stage and a third, cracked, stage up to failure (Figure2b). Failure, however, usually takes place, at lower load level, with slippage of the fabric within the matrix, that generally prevails on the tensile rupture of the fabric, at least in in SRG composites [6].

3. Experimental campaign

In the SRG system under investigation [5], fibres are made of Ultra High Tensile Stress Steel *UHTSS* cords, obtained by twisting two wires around three rectilinear ones at a short lay length to enhance interlocking with the mortar, having 0.108 mm^2 cross sectional area each. Wires are galvanized (coated with zinc) to provide rust protection and constitute a unidirectional fabric with fixed spacing between the ropes. They are attached to a fibreglass bidirectional mesh that facilitates handling and installation (Figure 3) and the product is packed in big coils from which cut-size sheets are obtained for specific applications.

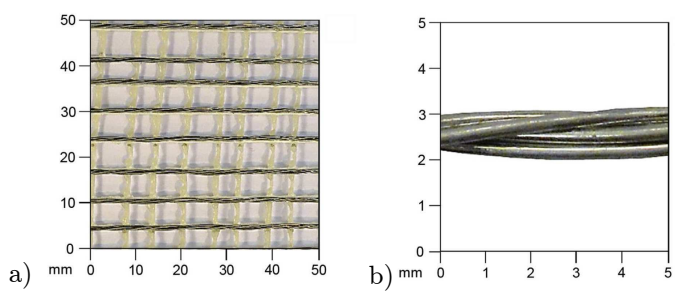

Figure 3: a) Textile and b) detail of the cord.

Table 1 summarizes some relevant manufacturing parameters, such as cord section A_{s1}, spacing i, equivalent thickness t and unit weight of the textile γ.

Table 1: Properties of *UHTSS* textile.

A_{s1} [mm^2]	i [mm]	t [mm]	γ [g/m^2]
0.534	6.35	0.084	670

A mineral-NHL mortar is used as matrix. Its compressive strength, elastic modulus, tensile strength and grain size range, are equal to 20.6 N/mm^2, 25 kN/mm^2, 3.75 N/mm^2 and 0-1.4 mm, respectively.

3.1. Clamping-grip tensile tests on dry textile

The tests on dry textiles were performed on six specimens made by eigth cords, having a nominal width of 50.8 mm, an average length of 436 mm [5]. The strips have been equipped with aluminium tabs at the ends and clamped in the wedges of the testing machine. Then the tensile tests have been performed, by applying the axial load in displacement control at a rate of 0.30 mm/min and recorded by a load cell. The measured stress and strains are reported in Figure 4 for the entire set; the curves show a linear phase, up to about the 60 to 80 % of the tensile strength and a hardening phase followed by failure with limited energy dissipation.

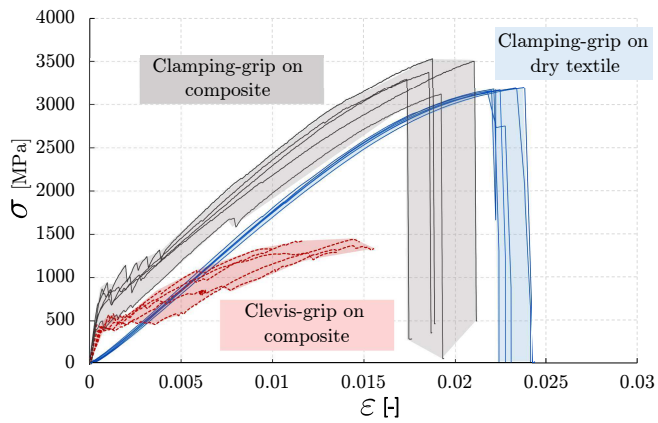

Figure 4: Experimental tests results on composite and dry textile specimens with clamping-grip and clevis-grip.

3.2. Clamping-grip tensile tests on the composite

A set of five clamping-grip tensile tests is considered, carried out in a previous work [5] on prismatic specimens having 600 mm length, 40 mm width, and 10 mm thickness. The embedded textile is made of five cords, corresponding to a nominal width of 31.75 mm and to an area of 2.67 mm^2. During the tests, axial load was applied in displacement control at a rate of 0.30 mm/min. Strains were recorded by an extensometer with 50 mm gauge length and by two linear potentiometers placed on the mortar by means of metallic plates over a gauge length of 200 mm.

Observing the clamping-grip test results reported in Figure 4 the three-staged response of the composite is clearly visible. The stiffening effect of mortar induces a strength increase of about 10% with respect to the dry textile accompanied by a slight larger dispersion of the response curves.

3.3. Clevis-grip tensile tests on the composite

The experimental results of clevis-grip tensile tests (Figure 2), where obtained from a previous experimental campaign [5]. The tested coupons have

500 mm length, 50 mm width and 13 mm thickness (eight cords are embedded in each specimen). Tests were performed using a universal screw-driven test frame with a capacity of 130 kN, under displacement control at a rate of 0.25 mm/min. Strains were measured using an extensometer over a 100 mm gauge length.

The response curves of the specimens are provided in Figure4. Despite the better bond between the twisted galvanized-steel cords and the mortar matrix [5], the specimen reaches failure because of fabric slippage. The applied displacement is accommodated, at the beginning, by the formation of multiple microcracks throughout the specimen length. After a longitudinal crack arises in the thickness of the specimen in correspondence with the gripping area, followed by a widening of the first horizontal crack closed to the steel tabs, when slippage of the textile inside the mortar matrix occurs. The quality of the mortar and its interlocking with textile and its spacing, are determinant in ensuring a proper bond that controls the mechanical behaviour.

Figure 4 provides a direct comparison of the three set of experimental tests previously described. This should be considered with some caution since, as highlighted in [9, 10], the load response might be influenced by the adopted rate.

4. Numerical modelling

A non-linear Finite Element numerical model has been used to reproduce and interpret the experimental results described in the previous section. SRG coupons were discretized into finite elements, using three-dimensional hexahedral elements for both, the mortar and the steel cords (Figure 5), while their interaction has been modelled through interfaces.

Numerical simulation has been conducted by applying a relative displacement in the y direction on the gripping areas at the two sides of the specimen. In case of clamping-grip setup, this phase follows a preliminary step in which a clamping pressure in the z direction, equal to 0.01 N/mm^2, is applied at both gripping areas of the coupon.

4.1. Constitutive models

According to the micromechanical modelling strategy adopted, SRG components are modelled as follows. Steel cords follow a ductile damage, combined with classical plasticity (Figure 6a), while mortar matrix behaves according to the Concrete Damaged Plasticity (CDP) model [16] (Figure 8). Materials are calibrated using the results of past experimental campaigns, as described in Section 3. The interface between mortar and cords is described according to a bilinear cohesive bond law (Figure 9).

4.1.1. Steel

The response (ε,σ) curve for steel under uniaxial tensile load (Figure6a) is characterized by an elastic branch up to the point b, a damage initiation

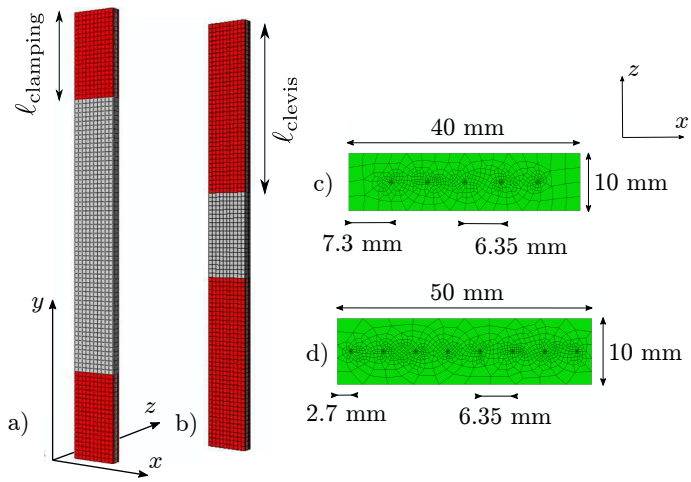

Figure 5: Finite element mesh for: a) clamping-grip setup ($\ell_{\text{clamping}} = 78$ mm) and b) clevis-grip setup ($\ell_{\text{clevis}} = 200$ mm). Transversal sections of the c) clamping-gripped specimen and d) clevis-gripped one.

criterion, in correspondence of point c, a damage evolution law (identified by the branch c-d).

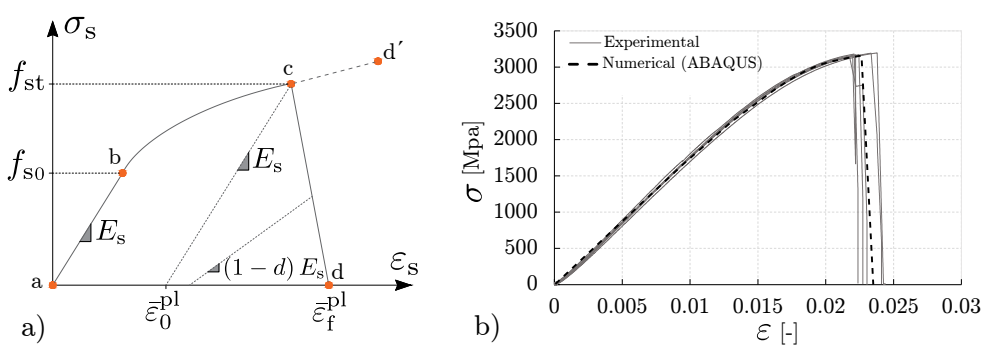

Figure 6: a) Adopted ductile damage constitutive law and b) numerical results for the single cord.

The elastic branch is defined by Young's modulus E_{s} and the yielding stress f_{s0}. Isotropic hardening characterizes the curve up to the onset of damage, in correspondence of the strength f_{st}.

To minimize mesh dependency issues, the damaged response is related to element dimensions and is therefore described in terms of equivalent plastic displacement $\bar{u}_0^{\text{pl}}$ or, identically, in terms of fracture energy G_{f}. In this case a linear damage evolution law is adopted and the fracture energy is referred to a characteristic length $L = 10$ mm. The adopted constitutive parameters are

reported in Table 2 and they have been calibrated on the average experimental response of the dry textile specimens.

Table 2: Steel parameters.

E_s [GPa]	f_{s0} [MPa]	f_{st} [MPa]	$\bar{\varepsilon}_0^{\mathrm{pl}}$	$\bar{\varepsilon}_{\mathrm{f}}^{\mathrm{pl}}$	G_{f} [N/mm]
182	1820	3157	0.0045	0.0234	9.57

Figure6b) shows the numerical simulation of the uniaxial tests on the steel cords in terms of stress and strain (dotted black line) together with the experimental response (solid grey line).

4.1.2. Mortar

Nonlinear response of mortar is described by the CDP [16], specifically formulated for isotropic brittle materials. The CDP accounts for different strength in tension and in compression and, assuming different damage parameters and evolution laws, the stress-strain relations are expressed by the following equations:

$$\sigma_{\mathrm{mc}} = (1 - d_{\mathrm{c}})\, E_{\mathrm{m}}\, (\varepsilon_{\mathrm{c}} - \tilde{\varepsilon}_{\mathrm{c}}^{\mathrm{pl}}) \tag{1}$$

$$\sigma_{\mathrm{mt}} = (1 - d_{\mathrm{t}})\, E_{\mathrm{m}}\, (\varepsilon_{\mathrm{t}} - \tilde{\varepsilon}_{\mathrm{t}}^{\mathrm{pl}}) \tag{2}$$

in which σ_{mt} and σ_{mc} are the uniaxial tensile and compressive stress, E_{m} is the initial elastic modulus, ε_{t} and ε_{c} are the total strains, $\tilde{\varepsilon}_{\mathrm{t}}^{\mathrm{pl}}$ and $\tilde{\varepsilon}_{\mathrm{c}}^{\mathrm{pl}}$ are the equivalent plastic strains in tension and in compression.

Mortar, like all brittle materials, is characterized by a strongly different behaviour in tension and compression. Nonetheless, its mechanical properties in compression do not play a significant role in the overall response, both experimentally and numerically. The tensile response of mortar, on the contrary, must be accurately described, since the formation and the development of cracks strongly influences the macroscopic behaviour of the composite.

The elastic branch is defined by two parameters, namely E_{m} and f_{mt} that, in the absence of direct experimental data on the mortar have been derived from the clamping-grip tensile tests on the composite coupons.

Assuming that, until the cracking point $(\varepsilon_{\mathrm{I}}, \sigma_{\mathrm{I}})$ the response is elastic and no slip occurs between the textile and the matrix, the following equilibrium equation holds:

$$E_{\mathrm{s}}\, A_{\mathrm{s}}\, \varepsilon_{\mathrm{I}} + E_{\mathrm{m}}\, A_{\mathrm{m}}\, \varepsilon_{\mathrm{I}} = N_{\mathrm{I}} \tag{3}$$

in which E_{s} is the steel Young's modulus, A_{m} and A_{s} are the net matrix area (397.32 mm^2) and the textile area (2.68 mm^2) respectively , and N_{I} and ε_{I} are the axial load and the strain at cracking. The mortar elastic modulus can thus be evaluated as:

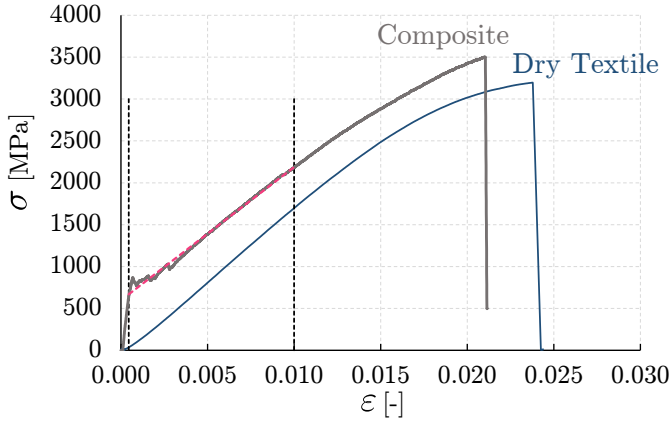

Figure 7: Average clamping-grip experimental curve (grey solid), average dry steel tensile response (blue) and composite response between cracking and yielding (dotted pink line) adopted in the calibration.

$$E_{\mathrm{m}} = \frac{N_{\mathrm{I}} - E_{\mathrm{s}}\, A_{\mathrm{s}}\, \varepsilon_{\mathrm{I}}}{A_{\mathrm{m}}\, \varepsilon_{\mathrm{I}}} \tag{4}$$

The post cracking branch of the mortar behaviour can be evaluated from the experimental tests (Figure 7), as the difference between the contribution of the FRCM coupon and that of the textile alone. Clearly this procedure provides a rough estimate, that includes tension stiffening, cracking of the mortar matrix etc.

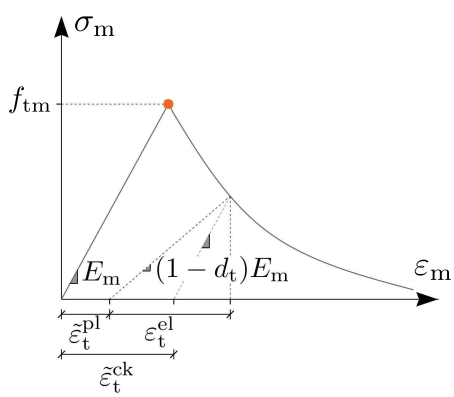

Figure 8: Concrete damaged plasticity model in tension.

As far as the steel behaves elastically, the stress contribution in the mortar can be calculated with the following expression:

$$\sigma_{\mathrm{m}}(\varepsilon) = \frac{N_{\mathrm{c}} - E_{\mathrm{s}}\, A_{\mathrm{s}}\, \varepsilon}{A_{\mathrm{m}}} \tag{5}$$

By repeating this calculation at different strain levels, between matrix cracking (ε_{I}) and steel yielding ($\varepsilon_{\mathrm{s}}(f_{\mathrm{s0}})$), the descending branch of the curve can be estimated. It is useful to point out that the postcracking behaviour of the mortar is described, in the framework of the concrete damaged plasticity model, in terms of stress and cracking strain $\tilde{\varepsilon}_{\mathrm{t}}^{\mathrm{ck}}$, related to the equivalent plastic strain by the following relation:

$$\tilde{\varepsilon}_{\mathrm{t}}^{\mathrm{pl}} = \tilde{\varepsilon}_{\mathrm{t}}^{\mathrm{ck}} - \frac{d_{\mathrm{t}}}{1 - d_{\mathrm{t}}}\, \frac{f_{\mathrm{t}}}{E_0} \tag{6}$$

4.1.3. Mortar-steel cohesive interface law

A fracture mechanics approach is followed for describing the behaviour at matrix-fibre interface, according to Mode II failure, through a bilinear bond-slip cohesive law, between the slip s and the corresponding tangential stress τ (Figure 9). The definition of the tangential stress τ_{m} at peak, the corresponding slip s_{m} and the slip value at debonding s_{deb} need to be identified in order to calibrate the $\tau - s$ relation [17, 18, 19, 20].

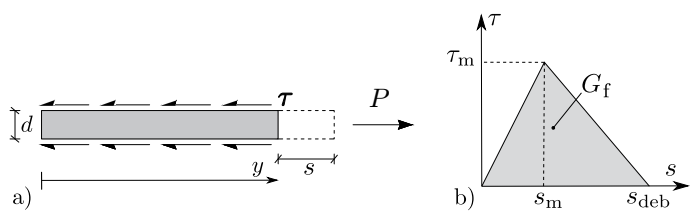

Figure 9: a) Free-body diagram of a segment of a steel cord and b) adopted bilinear bond-slip cohesive law.

In the present case, the values of the slips s_{m} and s_{deb} were assumed equal to those derived in previous works of the Authors [18, 21]. Conversely, the value of τ_{m}, in the absence of experimental results of pull-out tests, was estimated from experimental results of bond tests [5, 4], by assuming slippage of the steel cords inside the matrix. Assuming that the steel cords behaves elastically and the matrix can be considered as rigid, the load at debonding can be expressed as:

$$P_{\mathrm{deb}} = \frac{n}{2} \pi\, d \sqrt{2 E_{\mathrm{s}} G_{\mathrm{f}} d} \tag{7}$$

where n is the number of cords, d is the cord diameter, E_{s} is the Young's modulus of the steel cords and G_{f} is the fracture energy of the bond-slip cohesive law. Accordingly:

$$\tau_{\mathrm{m}} = \frac{4\, P_{\mathrm{deb}}}{n^2 \pi^2 d^3 E_{\mathrm{s}} s_{\mathrm{deb}}} \tag{8}$$

The parameters of the bond-slip law, deduced from the experimental database, are $s_{\mathrm{s}} = 0.005$ mm, $s_{\mathrm{deb}} = 1.1$ mm, $\tau_{\mathrm{m}} = 2.9\ N/\mathrm{mm}^2$.

5. Numerical results

In this section, the results of the numerical simulations of the direct tensile tests performed on SRG coupons with clamping-grip and clevis-grip setups are presented. In Figure. 10, the numerical outcomes in terms of global load-displacement curves are compared with the experimental ones. Figure 10a also reports the experimental and numerical results on dry textile strips. An overall good agreement between numerical and experimental results can be envisaged for both configurations. This proves the capability of the model to describe the tensile behaviour for the composite, under different boundary conditions.

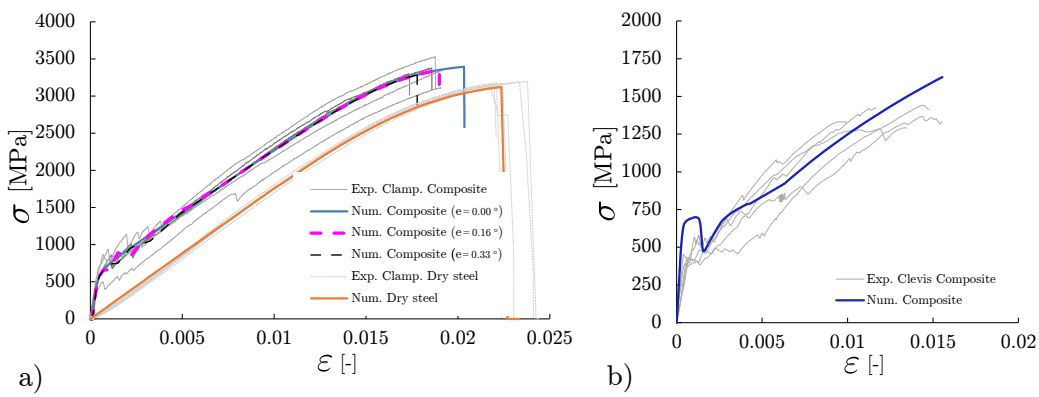

Figure 10: Numerical vs experimental results: global load-displacement response curves for direct tensile test on dry steel textile, on SRG coupons with a) clamping-grip setup and b) clevis-grip setup b).

Some sensitivity analyses have also been performed, introducing the effect of manufacturing imperfection. In the model, the inclination of the steel cords has been modified, by inducing a slight rotation of the fibres along the x axis equal to 0.16° and 0.33°. The analyses have shown that this imperfection induces a slight reduction in the attained ultimate strain at failure, that could explain the scatter in the experimental curves reported in Figure 10a.

Figure 11 reports the inelastic strain patterns in the mortar at two steps of the analysis, i.e. first crack formation (Figure 11a) and failure (Figure 11b) in case of clamping-grip setup. It is possible to observe that the first cracks occur at the bottom and at the top of the specimen, close to the gripping areas (Figure 11a). At failure, a stronger localization of inelastic strain in the same location can be observed, with a slight redistribution of cracks over the length of the coupon. Failure is reached through the tensile rupture of the steel cords in correspondence of the major cracks, as shown on the total strain distribution on the steel cords at failure (Figure 11c).

When the imperfection is introduced in the model, the initial crack pattern does not change (Figure 12a). However, at failure, the matrix displays several plastic strain localization bands. Due to eccentricity of the reinforcement with

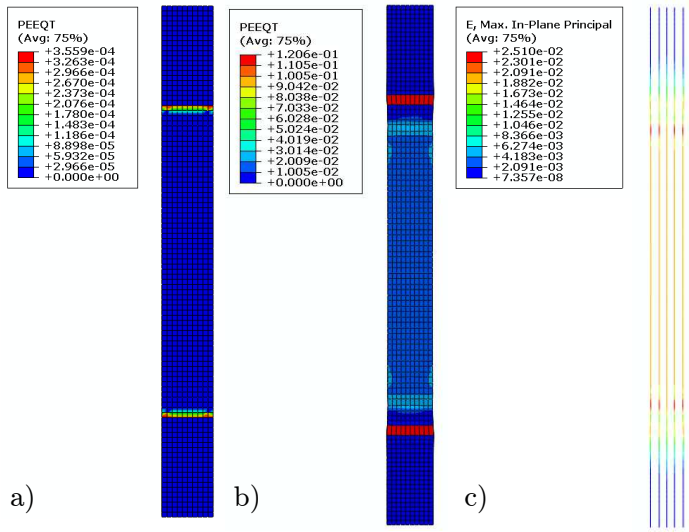

Figure 11: Tensile plastic strain patterns for mortar at a) crack initiation, b) failure point and total strain distribution along steel cords at failure c) for direct tensile test with clamping-grip setup.

respect to the thickness of the coupon, the inelastic strain pattern is different on the two faces of the specimens (Figure 12b-b′). This imperfection also induces a different strain pattern in the steel cords, such that failure is reached only in one section of the specimen, as shown in Figure 12c, according to experimental results (Figure 13).

In Figure 14b, the tensile damage pattern in case of direct tensile test on SRG coupon with clevis-grip setup is reported. The model succeeds in representing the localization of transversal cracks in the matrix right after the tab ends according to experimental failure configuration (Figure14a). Failure occurs through the slippage of the textile from the mortar matrix at the tab ends and this is controlled by the bond-slip law previously calibrated. The steel does not reach its ultimate tensile stress, reflecting in a lower value of the attained ultimate stress, both numerically and experimentally, since the ultimate load is lower than that of the dry textile.

Aiming at investigating the influence of the clamping with clevis-grip setup, numerical analyses were performed by varying the dimensions of the bonded length (ℓ_{clevis}) at the ends of the coupons. A strong dependence of the load capacity from the tab length is detected, showing an almost parabolic behaviour up to the effective bond length, over which no further load increase is attained.

Finally, Figure15 summarizes the strain at failure in steel cords in the case of clamping-grip (a) without and with imperfections and clevis grip (b) setups. The peak strain corresponds to the crack in the matrix, revealing the capacity of the model to capture the tension stiffening effect. The Figure also displays the

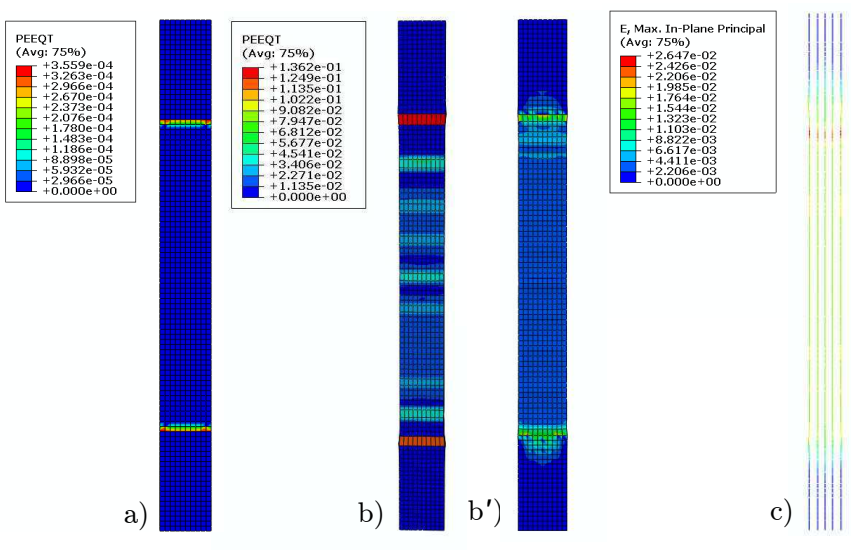

Figure 12: Tensile plastic strain patterns for mortar at a) crack initiation, at b) failure point front view and b′) back view and c) total strain distribution along steel cords at failure for direct tensile test with clamping-grip setup in case of inperfection.

large difference in the strain of the textile depending on the different gripping conditions.

6. Conclusions

In this work we presented the numerical simulations of two standardized test procedures that are commonly adopted to characterize SRG systems, made of steel cords embedded in inorganic matrix, that are widely used in structural applications.

After having briefly described the main technological aspects that characterize the test setups, some information on the experimental campaigns, constituting the benchmark data of this study, have been introduced. Material models calibration and boundary conditions have also been discussed. The results of the numerical analyses, observed in terms of damage patterns and stress distribution in the constituents, allow to recognize the influence of the gripping method on the test results.

The model is indeed capable of describing the mechanisms that control the tensile behaviour, namely the formation of cracks in the mortar and their widening, the ductile response of steel and the shear-slip at the interface.

In the case of clamping-grip test, the response (especially after the transition to the third stage) strongly depends on the steel tensile behaviour. This test gives information on the ultimate conditions of the constituents, but does not represent a faithful replication of the actual on-site installation conditions.

Figure 13: Experimental failure mode for tensile direct tests on SRG coupons in the case of clamping-grip setup.

The analyses have also aimed at investigating some aspects that can influence the behaviour, namely the effect of manufacturing imperfection of the specimens, that have been included by means of a given eccentricity of the cords. The non-planarity of steel does not only affect the tensile response in terms of the maximum attained deformation but also causes a different crack distribution along the coupon, in agreement with the experimental curves.

On the contrary, boundary conditions of clevis-grip tensile tests are more representative of SRG installation conditions, when the textile is not anchored to the substrate and the resisting mechanism is controlled by the shear bond at the textile-matrix interface. Though this class of composites can be involved in a number of failure modes, clevis-grip test provides a self-contained qualification procedure. However, a strong dependence of the test results on the bonded length of the tabs may affect the reliability of testing method.

The results of the numerical simulations are in satisfactory agreement with the experimental curves and some distinctive features of the response at failure are correctly represented, namely the tensile stress attained in the textile and the damage pattern in the matrix.

However, a series of aspects need to be further investigated. First, a more rigorous mechanical characterization of the mortar is needed, since the concrete damaged plasticity model has been calibrated through a semi-empirical process deriving the tensile response of the mortar from that of the composite. More accurate results could undoubtedly be achieved relying on a specific experimental characterization of the matrix. Second, since the imperfections have shown to play an important role in the response, other manufacturing defects are to be integrated in the model to provide a more reliable representation of the phenomenon.

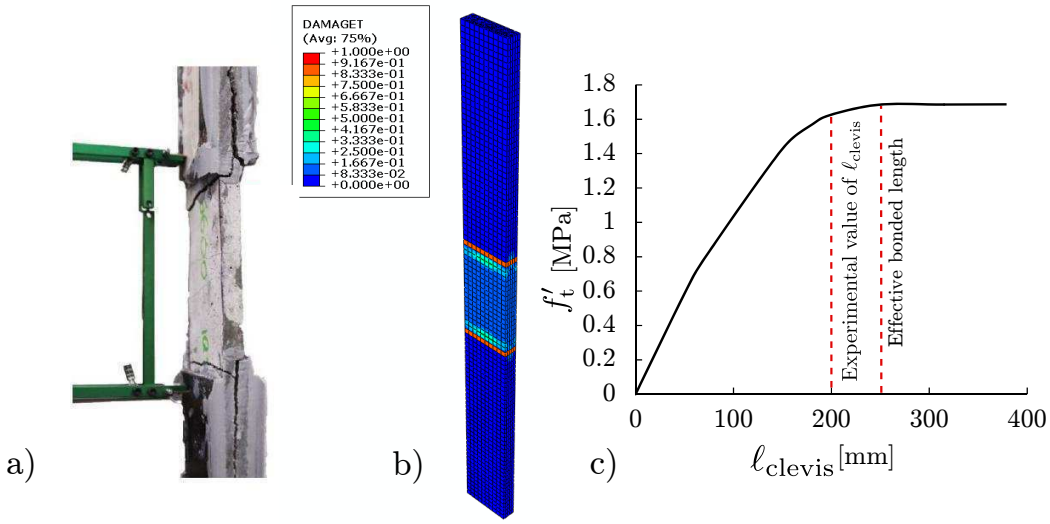

Figure 14: Experimental failure mode a) and tensile damage pattern for mortar at failure b) for direct tensile test with clevis-grip.

7. Acknowledgements

This work was supported by the Regione Lazio (SiCura 2018-2020 Research Grant) and by the ReLUIS 2019-2021 Research Project.

References

[1] Hegger, J., Will, N., Bruckermann, O. and Voss, S., 2006. Load–bearing behaviour and simulation of textile reinforced concrete. Materials and structures, 39(8), pp.765-776.

[2] Mobasher B, Peled A, Pahilajani J. Distributed cracking and stiffness degradation in fabric-cement composites. Mater Struct 2006;39(3):317-31.

[3] Contamine R, Si Larbi A, Hamelin P. Contribution to direct tensile testing of textile reinforced concrete (TRC) composites. Mater Sci Eng A 2011;528: 8589e98. http://dx.doi.org/10.1016/j.msea.2011.08.009.

[4] De Santis, S., Ceroni, F., de Felice, G., Fagone, M., Ghiassi, B., Kwiecień, A., Lignola, G.P., Morganti, M., Santandrea, M., Valluzzi, M.R. and Viskovic, A., 2017. Round robin test on tensile and bond behaviour of steel reinforced grout systems. Composites Part B: Engineering, 127, pp.100-120.

[5] De Santis, S., Hadad, H.A., De Caso y Basalo, F., De Felice, G. and Nanni, A., 2018. Acceptance Criteria for Tensile Characterization of Fabric-Reinforced Cementitious Matrix Systems for Concrete and Masonry Repair. Journal of Composites for Construction, 22(6), 04018048.

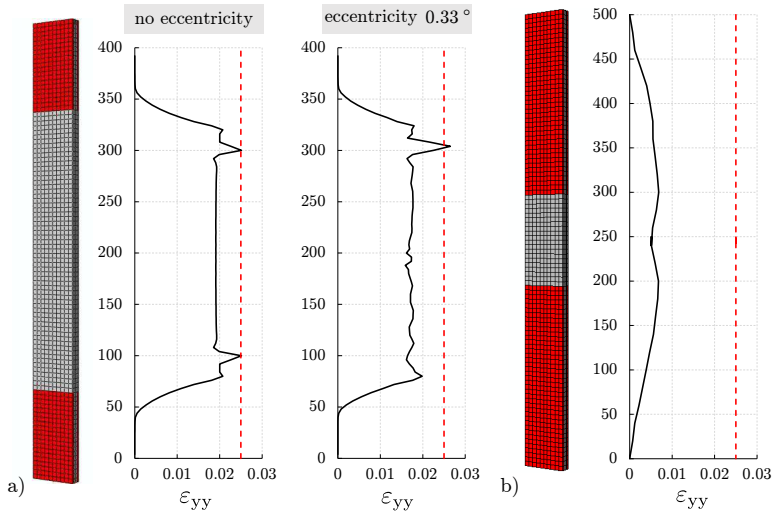

Figure 15: Total strain distribution along a steel cord at failure for a) clamping-grip setup and b) clevis-grip setup.

[6] Arboleda, D., Carozzi, F.G., Nanni, A. and Poggi, C., 2015. Testing procedures for the uniaxial tensile characterization of fabric-reinforced cementitious matrix composites. Journal of Composites for Construction, 20(3), p.04015063.

[7] Donnini J, Corinaldesi V, Nanni A. Mechanical properties of FRCM using carbon fabrics with different coating treatments. Compos Part B Eng 2016;38:220e8. http://dx.doi.org/10.1016/j.compositesb.2015.11.012.

[8] Hartig, J., Jesse, F., Schicktanz, K. and Häußler-Combe, U., 2012. Influence of experimental setups on the apparent uniaxial tensile load-bearing capacity of textile reinforced concrete specimens. Materials and structures, 45(3), pp.433-446.

[9] Carloni C, Verre S, Sneed LH, Ombres L. Loading rate effect on the debonding phenomenon in fibre reinforced cementitious matrix-concrete joints. Compos Part B Eng 2017;108:301-14.

[10] Yao, Y., Silva, F.A., Butler, M., Mechtcherine, V. and Mobasher, B., 2015. Tension stiffening in textile-reinforced concrete under high speed tensile loads. Cement and Concrete Composites, 64, pp.49-61.

[11] RILEM Technical Committee 232-TDT (Wolfgang Brameshuber) brameshuber@ ibac. rwth-aachen. de, 2016. Recommendation of RILEM TC 232-TDT: test methods and design of textile reinforced concrete: Uniaxial tensile test: test method to determine the load bearing behavior

of tensile specimens made of textile reinforced concrete. Materials and Structures, 49, 4923–4927.

[12] ACI 434. Acceptance criteria for masonry and concrete strengthening using fabric-reinforced cementitious matrix (FRCM) and steel reinforced grout (SRG) composite systems, 2016.

[13] Hartig, J., Häußler-Combe, U. and Schicktanz, K., 2008. Influence of bond properties on the tensile behaviour of Textile Reinforced Concrete. Cement and concrete composites, 30(10), pp.898-906.

[14] B. Mobasher, J. Pahilajani, A. Peled, Analytical simulation of tensile response of fabric reinforced cement based composites, Cem. Concr. Compos 28 (2006) 77-89, http://dx.doi.org/10.1016/j.cemconcomp.2005.06.007.

[15] Soranakom C., Mobasher B., Modeling of tension stiffening in reinforced cement composites: Part I. Theoretical modeling. Materials and Structures (2010) 43:1217–1230. DOI 10.1617/s11527-010-9594-8

[16] Lee, J. and Fenves, G.L., 1998. Plastic-damage model for cyclic loading of concrete structures. Journal of engineering mechanics, 124(8), 892–900.

[17] Malena, M., Focacci, F., Carloni, C. and De Felice, G., 2017. The effect of the shape of the cohesive material law on the stress transfer at the FRP-masonry interface. Composites Part B: Engineering, 110, pp.368-380.

[18] Malena, M. and de Felice, G., 2014. Debonding of composites on a curved masonry substrate: Experimental results and analytical formulation. Composite Structures, 112, 194–206.

[19] Ceroni, F., de Felice, G., Grande, E., Malena, M., Mazzotti, C., Murgo, F., Sacco, E. and Valluzzi, M.R., 2014. Analytical and numerical modeling of composite-to-brick bond. Materials and structures, 47(12), pp.1987–2003.

[20] D'Antino, T., Carloni, C., Sneed, L.H. and Pellegrino, C., 2014. Matrix–fiber bond behavior in PBO FRCM composites: A fracture mechanics approach. Engineering Fracture Mechanics, 117, 94–111.

[21] Malena, M., 2018. Closed-form solution to the debonding of mortar based composites on curved substrates. Composites Part B: Engineering, 139, 249–258.